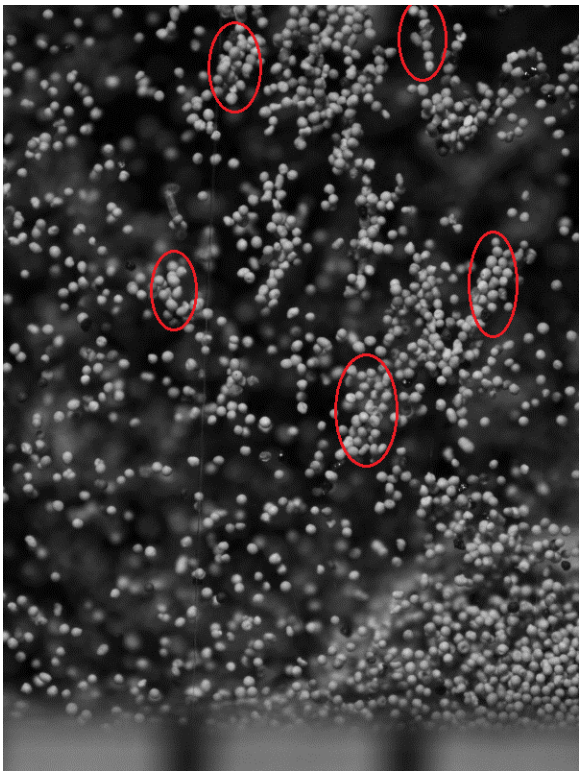

Experimental study and discrete element method simulation of Geldart Group A particles in a small-scale fluidized bed

Tingwen Li[a,b*], Swapna Rabha[a], Vikrant Verma[a], Jean-François Dietiker[a,c], Yupeng Xu[a], Liqiang Lu[a], William Rogers[a], Balaji Gopalan[a,c], Greggory Breault[a,e], Jonathan Tucker[a,d], Rupen Panday[a,e]

a. National Energy Technology Laboratory, Morgantown, WV 26505, USA

b. AECOM, Morgantown, WV 26505, USA

c. West Virginia University Research Corporation, Morgantown, WV 26506, USA

d. West Virginia University, Morgantown, WV 26506, USA

e. REM Engineering Services, Morgantown, WV 26506, USA

Abstract

Geldart Group A particles are of great importance in various chemical processes because of advantages such as ease of fluidization, large surface area, and many other unique properties. It is very challenging to model the fluidization behavior of such particles as widely reported in the literature. In this study, a pseudo-2D experimental column with a width of 5 cm, a height of 45 cm, and a depth of 0.32 cm was developed for detailed measurements of fluidized bed hydrodynamics of fine particles to facilitate the validation of computational fluid dynamic (CFD) modeling. The hydrodynamics of sieved FCC particles (Sauter mean diameter of 148 μm and density of 1,300 kg/m^3) and NETL-32D sorbents (Sauter mean diameter of 100 μm and density of 480 kg/m^3) were investigated mainly through the visualization by a high-speed camera. Numerical simulations were then conducted by using NETL's open source code MFIX-DEM. Both qualitative and quantitative information including bed expansion, bubble characteristics, and solid movement were compared between the numerical simulations and the experimental measurement. The cohesive van der Waals force was incorporated in the MFIX-DEM simulations and its influences on the flow hydrodynamics were studied.

Keywords: discrete element method, fluidized bed, Group A particles, bed expansion, cohesive force, high-speed image

* Corresponding author at: National Energy Technology Laboratory,

Morgantown, WV 26505, USA. Tel.: 1 304 285 4538.

E-mail addresses: tingwen.li@contr.netl.doe.gov, litingwen@gmail.com (T. Li).

1. Introduction

Small particles classified by Geldart as Group A powders are of great importance in various chemical processes owning to advantages such as ease of fluidization, large surface area, and many other unique properties [1]. For example, Group A particles demonstrate a unique feature of uniform expansion after minimum fluidization and prior to bubbling. This property of homogeneous expansion tends to maintain Group A particles at aerated state longer hence facilitates easier circulation and better mixing of gas and solids [1]. In addition, a maximum bubble size has been observed experimentally for Group A particles in fluidized beds when bubble coalescence and breakup reach an equilibrium [1]. Compared to Group B particles, this feature promotes the gas-solids mixing and minimizes the gas bypassing by large bubbles. All these desirable fluidization characteristics make Group A particles preferential in many industrial processes. One of the most important examples is the fluid catalytic cracking (FCC) process in which the FCC particles are used to convert the high-boiling, high-molecular weight hydrocarbon fractions of petroleum crude oils to more valuable gasoline, olefinic gases, and other products. Typical FCC particles have a bulk density of 0.8 to 0.96 g/cm^3 and a particle size distribution ranging from 10 to 150μm and average particle size of 60 to 100μm.

Extensive experimental work has been reported on the fluidization behavior of group A particles, especially for FCC particles [2–5]. With the continuous evolvement of computer hardware and development of theory and numerical algorithm, computational fluid dynamics (CFD) has been demonstrated a complementary tool to experiment to investigate gas-solid flow in multiphase systems [6]. So far two major approaches are being used to model gas-solid fluidization systems, i.e**.** the Eulerian–Eulerian (EE) method (also called the two-fluid model or TFM), and the Lagrangian–Eulerian (LE) method. The former treats both gas and solid phases as interpenetrating continuum with appropriate constitutive correlations. Additional constitutive closures are usually developed based on the kinetic granular theory to model the solids phase as a continuum [7]. The latter treats the gas phase as a continuum, but tracks the solid phase at the particle level by solving the trajectory of each individual particle (e.g. discrete element method (DEM)) or a swarm of particles (e.g. particle-in-cell (PIC) method) [8,9]. Both EE and ~~E~~LE models have been applied to model the flow in fluidized-bed reactors involving Geldart A particles, and with varying degrees of success. Due to the expensive computational cost, CFD-DEM simulations of group A particles are typically limited to extremely small systems with the focus on the fundamental aspects such as minimum fluidization velocity and the effect of cohesive force [10]. For validation against real fluidized bed systems of fine particles, most simulations were performed based on the EE approach.

It has been widely reported that the TFM substantially over-predicts the bed expansion of Geldart A particles in bubbling fluidized beds [11–14]. As the interphase drag force plays the key role in affecting bed expansion, different methods have been proposed to adjust the drag model through an *ad hoc* scale factor [11,13], matching the minimum fluidization velocity [12]

or using an effective agglomerate size [15,16]. Wang et al. suggested that the over-prediction of bed expansion is mainly attributed to the small heterogeneous structures, i.e. small bubbles, cluster, or agglomerates which are not resolved in the numerical simulation with relatively coarse grids [17]. They demonstrated that TFM could predict the correct bed expansion, without any artificial modifications, provided that sufficiently fine grid size and small time step were used by comparing against DEM simulations of group A particles. Consequently, one has to use fine grid and small time step to resolve the heterogeneous structures with small spatial and temporal scales. Instead of using an extremely fine grid, many sub-grid drag modifications have been developed to account for the effect of small unresolved scales on the resolved mesoscales in dense gas-particle flows using a coarse grid with promising results [18–20]. However, recent studies tend to suggest that the grid refinement of TFM simulation to even less than particle diameter cannot fully overcome the over-prediction of bed expansion of group A particles [14,21]. Since Wang et al.'s work was based on the comparison of fine-grid TFM simulation with the DEM simulations [17], it is important to validate the DEM simulations against experiments for modeling Group A particles.

Early DEM studies of Geldart Group A particles mainly focued on the effect of cohesive force between particles, such as van der Waals force, in two-dimensional (2D) systems [10,22–27]. A major difference of Group A particles to Group B and D particles is the strong inter-particle cohesive force which becomes significant when the particle size is small [28]. It is straightforward to account for the cohesive force, i.e. van der Waals force, in DEM simulations. However, it has been shown that the stiffness of spring constant used in the DEM simulation has a significant effect on the fluidization behavior when the cohesive force is accounted for [29]. A dynamic adhesion force model was proposed to incorporate the effect of spring constant used in DEM model by Kobayashi et al. and the simulation results were qualitatively validated against a pseudo-2D fluidized bed with respect to bubbling behavior using a 2D simulation [30]. Similarly, Gu et al. proposed a modified cohesion model for Group A and C particles [31]. The model was verified using a small three-dimensional (3D) fluidized bed with periodic boundary conditions. Galvin and Benyahia conducted 3D DEM simulations of Group A particles to investigate the effects of cohesive forces of van der Waals type in the fluidization/defluidization of Group A particles with respect to some design-significant parameters including minimum fluidization and bubbling velocities [32]. They reported that the cohesive forces contributed to the commonly observed phenomena, such as pressure overshoot and hysteresis around minimum fluidization. Liu et al. investigated the defluidization of fine cohesive particles via small-scale DEM simulations and experiments [33]. They reported that the simulation results for cohesive particles were sensitive to particle stiffness and static bed height. A quantitative validation was then conducted between small-scale simulations and lab-scale experiments in terms of the complete fluidization velocity.

As suggested in the above literature survey, very limited validation studies of DEM simulations for Group A particles have been reported. This is mainly due to the prohibited computational

cost required by tracking a large number of particles typically found in even a small laboratory facility. In the current work, a small-scale pseudo-2D fluidized bed was constructed for testing of different Group A particles. CFD-DEM simulations were conducted to validate the numerical model by comparing with the bed expansion and bubble properties extracted from the experimental images.

2. Experiment Setup

A small pseudo-2D column made of plexiglass was built at National Energy Technology Laboratory (NETL), Morgantown for visualization of the fine particle flow using a high-speed camera (Fastec Imaging Inc), which has the capacity to capture at 500 fps with resolution of 1208x1000. Figure 1 shows the schematic and a picture of the experimental setup which has dimensions of 0.32 cm in thickness and 5 cm in width and 45 cm in height. A sintered metal porous plate (Mott corporation; media grade 5) was used as the gas distributor which provided sufficiently high pressure-drop and uniform gas flow distribution.

Figure 1. (a) Schematic and (b) picture of the experimental setup

Two types of Geldart A particles were tested in the current facility. The first type of particles investigated was sieved spent FCC particles which have a narrow particle size distribution with Sauter mean diameter of 148 µm and particle density of 1300 kg/m^3. Another type of group A particles tested was NETL-32D sorbent which is an amine-impregnated mesoporous sorbent for CO_2 capture [34,35]. The NETL-32D sorbents have a Sauter mean diameter of 100 µm and particle density of 480 kg/m^3 with the sphericity of 0.89. Physical properties for both types of particles were characterized followed the methodology outlined by Tucker et al. [36]. Nitrogen under ambient conditions was used to fluidize both types of particles. The minimum fluidization velocities for FCC particles and NETL-32D sorbent were measured as 1.73 cm/s and 0.23 cm/s, respectively. The back light and front light were used in the experiment to facilitate bubbling tracking and particle tracking respectively. The images of the bubbly flow in the fluidized bed were captured by a high-speed camera at a spatial resolution of 718 x 892 pixels with physical dimension of 6 cm x 7.5 cm right above the distributor and a temporal resolution of 700 frames per second for 14 seconds. These images were used for both qualitative and quantitative validation of the results predicted by open-source MFIX-DEM code for the same operating conditions. In addition, particle tracking was conducted through in-house developed high-speed PIV [37], which will be reported in the future study for further validation.

3. Modeling approach

The open-source MFIX-DEM code, developed at US Department of Energy's National Energy Technology Laboratory (NETL) was used to conduct the numerical simulations [38]. In MFIX-DEM, DEM for the solid particles is coupled with the gas flow solver to simulate the gas-solid flow. For DEM, the inter-particle collisions are directly resolved using a soft-sphere model based on a linear spring-dashpot model which treats the collision as a continuous process taking place over a finite time [39]. The contact force is then calculated as a function of the distance between colliding particles based on physically realistic interaction laws using empirical spring stiffness, dissipation constant, and friction coefficient. The particle–wall interaction is treated in the same way as the particle–particle collision. The gas flow is simulated by solving the averaged Navier-Stokes equations for mass and momentum conservation which account for solid volume fraction and additional coupling terms due to interactions between the two phases [40]. The implementation of MFIX-DEM has been verified and validated for non-cohesive particles [41,42].

The particles were modeled as a mono-dispersed system with the mean particle size and density being used. The numerical parameters used in the simulations are summarized for simulations of both types of particles in Table 1. The ratio between grid size and particle diameter was about 4 for both types of particles based on the previous studies [41,43]. The distributor was treated as an inflow boundary condition with uniform gas velocity distribution. This is believed a reasonable assumption as the pressure drop through the distributor has been measured to be much greater than the bed weight being tested. A pressure outlet was used at the top and no-slip wall boundary conditions were used for all the walls. A free-slip wall boundary condition for the gas phase was also tested for the front and back walls to evaluate the impact on the numerical results which shown only negligible effect as the particle-wall interaction dominated. The Gidaspow drag model which is a combination of the empirical Ergun equation and Wen & Yu model was used for the gas-solid coupling [7]. The simulations were run in a hybrid parallel mode (MPI + OpenMP) which makes the simulation of millions of particles affordable [44,45]. The simulations typically took from one to two weeks on a high performance computer using 256 CPUs.

Table 1. Numerical parameters used in the simulations.

To account for the cohesive inter-particle force, the van der Waals force was incorporated into the simulation as [46]

$$F_{vdw} = \frac{Ar}{12s^2}$$

where A is the Hamaker constant which depends on the material properties, r is the particle radius and s is the separation of particle surfaces. A minimum separation corresponding to the intermolecular spacing was used in the calculation to avoid the singularity of van der Waals

force as the particle separation approaching zero. In addition, a cut-off separation was assumed beyond which the van der Waals force is ignored. Hence the van der Waals force experienced by the particle can be modeled as

$$F_{vdw} = \begin{cases} 0 & s > s_{max} \\ \dfrac{Ar}{12s^2} & s_{min} < s \le s_{max} \\ \dfrac{Ar}{12s_{min}^2} & s \le s_{min} \end{cases}$$

In the numerical simulations, 4 nm and 50 μm were used for the minimum and cut-off separations, s_{min} and s_{max}, respectively.. Similar model was used for the particle-wall interaction. This type of cohesive force model has been successfully utilized by Galvin and Benyahia to study the effect of cohesive forces on the fluidization of group A particles [32].

Field Code Changed

Field Code Changed

4. Results and discussion

FCC particles

Experiments were conducted for different static bed heights (6 cm and 11 cm) and superficial gas velocities (U = 2, 3, 5 and 7 Umf). However, for the current validation study, only cases with a static bed height of 6 cm were considered which resulted in 3.2 million particles in the simulations. Figure 2 shows experimental images for superficial gas velocities of 2Umf, and 5Umf using the backlighting coving the width of the experimental column with free-board excluded. As can be seen from the experimental images, the bubbles span through the bed thickness and can be easily identified.

Figure 2. Raw images of bubbling fluidized bed of FCC particles with superficial gas velocities of (a) 2Umf; (b) 5Umf (static bed height: 6 cm).

The simulations were carried out for three superficial gas velocities (2 Umf, 3 Umf, and 5 Umf) for 5 seconds. The flow reached fully developed state in less than 1 second. The results afterward were analyzed for validation against the experimental data. For comparison, two snapshots of central slice of numerical results are shown in Figure 3 for superficial gas velocities of 2Umf and 5Umf, respectively. The MFIX-DEM simulations are capable of capturing the qualitative bubbling behaviors. Consistent with the experimental observation, larger bubbles are formed under high superficial gas velocity and more vigorously coalescence are predicted. However, there do exist differences in the pattern of bubble formation near the distributor plate. For example, bubbles tend to form near the left and right walls in the simulation but rarely in the

central region due to a strong solid downflow there for the case with 2 Umf as indicated in Figure 3(a) by the red arrow. Such a strong solid downflow was not observed in the experimental test and bubbles could form throughout the distributor with a slightly stronger tendency in the near wall regions. In addition, the bubble interface predicted by the simulation is smoother than that observed from the experimental video. Such a difference is partially attributed to the direct comparison of the numerical voidage/solid volume fraction distribution to the experimental picture without a reliable correlation between the 2D image intensity and the true solid concentration [47]. On the other hand, the DEM simulations without accounting for the cohesive forces fail to capture ~~large~~ agglomerates raining down through the bubble top surface as will be discussed next.

Figure 3. Snapshots of numerical simulations of FCC particles with superficial gas velocities of (a) 2Umf; (b) 5Umf (static bed height: 6 cm).

The effect of van der Waals force was included in the simulation by setting different values for Hamaker constant to achieved the desired ratio of maximum cohesive force, $F_{vdw,\max}$, to particle weight, W_p. Figure 4 shows snapshots of numerical results for different strengths of van der Waals force corresponding to $F_{vdw,\max}/W_p$ = 0, 5, 10, and 20 for the case with a superficial gas velocity of 5 Umf. Both views along the centerline slice and on the front wall are shown. When the cohesive force is included, it is observed that a layer of particles tends to form stablely along the wall as can be seen in Figure 4(b) for cases with high cohesive forces. The cohesive force also helps overcome the down flow in the center as shown in Figure 3(a) and tends to predict uniform bubble formation near the distributor. In addition, when a very high cohesive force is used, particles start to form large agglomerates in the dense region. Those agglomerates are broken up by the gas flow in the form of cracks along the bubble surface as can be seen in Figure 4(a) for $F_{vdw,\max}/W_p$ =20.

Field Code Changed

Figure 4. Effect of cohesive force on the instantaneous bubbling behavior of FCC particles under 5Umf for (a) central slice and (b) the front wall ($F_{vdw,\max}/W_p$ = 0, 5, 10, and 20 from left to right).

In the current DEM simulations, a low spring constant of 5 N/m is used for particle-particle and particle-wall contact to allow for large time-step. This is a routine exercise for DEM simulations to compromise between speed and accuracy. For gas-solids fluidized bed simulations, it has been demonstrated that the flow prediction is insensitive to the spring constant for non-cohesive particles [40]. However, the stiffness of spring constant used in the DEM simulation has a significant impact on the fluidization behavior when the cohesive force is accounted [29]. To accurately capture the effect of cohesive force, the realistic particle stiffness should be used

which is infeasible at the current stage. Otherwise, the dynamic adhesion force models by Kobayashi et al. [30] or Gu et al. [31] should be used which effectively reduce the cohesive force for low particle stiffness. According to those cohesion models, the current simulation of $F_{vdw,\max}/W_p = 5$ with the particle stiffness of 5 N/m should correspond to $F_{vdw,\max}/W_p = 50$ with the particle stiffness of 500 N/m and even higher for the realistic particle stiffness. It is unlikely that the FCC particles have such a strong cohesive force. Surprisingly, as far as the bubbling behavior is concerned, the results of $F_{vdw,\max}/W_p = 5$ do not show noticeable difference comparing to those for non-cohesive particles as shown in Figure 4. Simply including the van der Waals force in contact force calculation does not change the result of the current FCC system much. It is also worth noting that DEM simulations with modified cohesion model to account for the effect of low particle stiffness are very close to those of non-cohesive particles [30,48]. This tends to suggest that either the cohesive force is insignificant for the current system or only accounting for it in DEM particle interaction is not sufficient. In the following discussion, it will be shown that the cohesive force has significant effect on the detailed flow behavior in the current system.

The sieved FCC particles fall close to the boundary of group A/B according to the Geldart's particle classification. It is expected that the role of van der Waals force should be less critical comparing to the typical group A particles [49]. In order to observe particle-particle interaction, high-resolution images with a small field of view of the bubbling fluidized bed were captured at a spatial resolution of 600x800 pixels and temporal resolution of 1000 frame per second. Figure 5 shows four consecutive snapshots of particle-particle interaction at the superficial gas velocity of 5 Umf. A few possible agglomerates are identified and highlighted in Figure 5(a) and their movements can be seen in the subsequent figures. These agglomerates are not permanent, and they continuously form and breakup inside the bed. The agglomerates observed in the experimental test are attributed to the cohesive force either due to electro-static or van der Waals force. In addition, humidified gas with a small amount of larostat addition was used in the test to reduce the electro-static effect. The addition of larostat tended to cause additional interparticle capillary force. It should be noted that the van der Waals force and interparticle capillary force share the similar cohesive characteristics. Hence the cohesive force implemented in the MFIX-DEM simulation should be capable of reproducing the agglomerates observed experimentally. By including the cohesive force in DEM simulations, different agglomerate behaviors were observed. The cohesive force experienced by each particle is used to help identify agglomerates in the numerical simulations as shown in Figure 6 where particles with non-zero cohesive force are shown in black and the rest particles are shown in gray. In Figure 6, close view of particles in the bubble region are shown to visualize the agglomerates. For simulation with $F_{vdw,\max}/W_p = 5$, most particles are dispersed in the bubble region and only small agglomerates can be occasionally observed. As the strength of cohesive is increased, large agglomerates with many particles tend to be predicted in the simulations as shown in Figure 6(b) and Figure 6(c). The DEM simulations with cohesive force are capable of predicting the agglomerate phenomenon observed in the experimental tests. However, the agglomerates predicted in simulations tend to

Field Code Changed

be larger and with smaller aspect ratio comparing to the experimental observation. ~~Such agglomerates cannot be observed in the simulations even with the highest strength of cohesive force.~~ With that, it is suspected that simply including van der Waals force in particle contact is not sufficient to accurately predict particle agglomerates. The formation of agglomerates, especially the typical elongated shape agglomerates as observed in the current experimental study, is believed to be closely related to the gas-particle interaction with the presence of cohesive interparticle forces. However, such small-scale gas-solid interaction is beyond the capability of current CFD-DEM approach and can only be captured by direct numerical simulations.

Figure 5. Pictures taken for FCC particles with 5Umf (time interval between images is 0.002 second).

Figure 6. Snapshots of DEM simulations characterizing agglomerates formation for different strengths of cohesive force (a) $F_{vdw,\max}/W_p$ = 5, (b) $F_{vdw,\max}/W_p$ = 10, (c) $F_{vdw,\max}/W_p$ = 20.

Field Code Changed
Field Code Changed
Field Code Changed

Table 2 compares the predicted bed heights with the experimental measurements for different superficial gas velocities. The bed heights were measured based on the animation or video from simulation and experiment through image processing. The uncertainties increase with the gas velocity as the bed surface vigorously fluctuates for high flow rates. The numerical results shown for comparison are based on the DEM simulation of non-cohesive particles. Overall, the agreement is good for the bed expansion. No over-prediction in bed height is observed for all cases. Including the cohesive force slightly increase the bed expansion for both operating conditions.

Table 2. Comparison of bed expansion for FCC particles with a static bed height of 6 cm predicted by CFD-DEM simulation of non-cohesive particles.

The bubble size information was extracted from central slices of the transient simulation using a threshold voidage of 0.8. Detailed information on the procedure for image processing and bubble statistics can be found in [50]. Consistent approaches were used for analyzing both simulation results and experimental images. For the experimental results, bubbles intersecting with the lower and upper bounds of the view were excluded which leads to lower measured bubble sizes in those regions. In addition, the experimental results did not cover the whole bed height as the free-board region was excluded in the experimental video using backlighting. Figure 7~~Figure 6~~ shows the comparison of bubble size variation along the height. The numerical simulations tend

to over-predict the bubble size compared with the experimental measurements. On the other hand, the simulations predicted the variation of bubble rising velocity with respect to the bubble diameter reasonably well as shown in Figure 8~~Figure 7~~. As mentioned above, it is not straightforward to directly compare the experimental digital image to simulation results. Hence, further in-depth analysis is needed for the validation of bubble properties which will be reported in the future study.

Figure 7. Comparison of bubble diameter along the bed height for (a) 2 Umf; (b) 3 Umf; (c) 5 Umf (error bar corresponds to the standard deviation, numerical results are for non-cohesive particles)

Figure 8. Comparison of vertical bubble velocity as a function of bubble diameter for (a) 2 Umf; (b) 3 Umf; (c) 5 Umf (error bar corresponds to the standard deviation, numerical results are for non-cohesive particles)

The effect of the cohesive force on the bubble properties are examined as shown in Figure 9~~Figure 8~~. For different strengths of van der Waals force, there are only marginal impact on the predicted bubble sizes and velocities. For the case with the strongest cohesive force, $F_{vdw,\max}/W_p$ = 20, the bubble properties show the most deviation from the rest. It should be noted that for that case the cohesive force is so strong that some challenging behaviors start to take place which is very different from the experimental observation. Through this comparison, it suggests that within certain range the cohesive inter-particle force has only negligible effect on the bubble characteristics.

Figure 9. Effect of cohesive force on (a) mean bubble diameter along the bed height and (b) vertical bubble velocity as a function of bubble diameter for the case of 5 Umf.

NETL--32D Sorbents

Different bed heights and superficial gas velocities were tested for the NETL--32D sorbents. To reduce the computational cost of the simulation, the current study focuses on tests with low static bed height of 3.8cm. Figure 8 shows two images of the experimental tests with superficial gas velocities of 1.5 cm/s and 2.5 cm/s, respectively. It should be noted that these images were taken with front-lighting hence the colors of bubble and solid emulsion are different from those for FCC particles. The vigorous bubbling behaviors were observed for both conditions where bubbles rise upward with continuously splitting and coalescing. The flow patterns for both operating conditions are similar and the expended bed heights were measured the same about 5.4 cm.

Figure 10. Experimental images of NETL-32D sorbent particles with superficial gas velocity of (a) 1.5 cm/s; (b) 2.5 cm/s.

The static bed height of 3.8 cm was simulated for NETL-32D sorbents which led to 7.2 million particles in the system. Physical properties and numerical parameters summarized in Table 1 were used in the simulations. Due to the large number of particles needed to be simulated, only a few simulations were conducted for NETL-32D sorbents fluidized at a superficial gas velocity of 2.5 cm/s. Again the effect of cohesive force was examined by assigning different strengths of van der Waals force for particle-particle and particle-wall contacts.

Figure 11~~Figure 10~~ shows views of central slice and front wall for simulations with different strengths of van der Waals force corresponding to $F_{vdw,\max}/W_p$ = 0, 5, 10. Consistent with the FCC results presented above, the strong cohesive force simulated lead to particles adhering to the walls. As a result, the voidage distributions along the front wall differ significantly from those along the central slice. Comparing to FCC particles, the numerical results of NETL-32D sorbents shows a stronger effect from the cohesive force for the same $F_{vdw,\max}/W_p$.

Figure 11. Effect of cohesive force on the instantaneous bubbling behavior of NETL-32D sorbent particles with a superficial gas velocity of 2.5 cm/s for (a) central slice and (b) front wall ($F_{vdw,\max}/W_p$ = 0, 5, 10 from left to right).

The presence of strong cohesive force increases the wall friction to the solid flow hence alters the solid circulation pattern substantially. To demonstrate the profound impact of cohesive force on the flow behavior, the mean voidage distributions along the central slice are shown in Figure 12~~Figure 11~~ for non-cohesive and cohesive cases together with the gas velocity vectors. A strong vortex was predicted for the solid flow in the non-cohesive simulation as indicated in Figure 12~~Figure 11~~(a). Such a persistent solid circulation pattern was not observed in the experiment. The inclusion of cohesive force increases the solid viscosity and wall friction, therefore leads to less vigorous solid circulation which is more consistent with the experimental observation. Similar but not less impact on the solid circulation pattern was observed for the FCC particle simulations presented above.

Figure 12. Distribution of mean voidage and gas velocity vectors along the central slice (a) $F_{vdw,\max}/W_p$ = 0; (b) $F_{vdw,\max}/W_p$ = 5.

It should be noted that NETL- ~~the~~ 32D particles ~~is~~are smaller and lighter than the FCC particles. Hence the ratio between cohesive force and particle weight is ~~much~~ expected to be higher in reality for NETL-32D sorbents than FCC particles assuming the strengths of cohesive force~~s~~ are comparable. The experimental observation did confirm the numerical prediction on the effect of cohesive force. A close view of the experimental test of NETL-32D sorbents is shown in Figure 13~~Figure 12~~(a) where the layer of particles sticking on the wall can be seen even with the presence of bubble. No successful measurements on bubble properties were available from the experimental tests for NETL- ~~the~~ 32D sorbents mainly due to the layer of particles sticking on the wall. The photomicrograph of NETL-32D sorbent particles is shown in Figure 13~~Figure 12~~(b) in which the irregular particle shape and semi-transparent nature can be seen. The semi-transparent nature of NETL-32D sorbent particles made the visualization of particle agglomeration very difficult.

Figure 13. Close view of the experimental test of NETL-32D sorbents with a superficial gas velocity of 2.5 cm/s with dark color indicates high voidage (a) and photomicrograph of NETL-32D sorbent particles (b).

Due to the limited quantitative information available from the experimental tests of NETL-32D sorbents, only the bed expansions predicted from the simulations were compared against experiment. The numerical prediction of bed height for the superficial gas velocity of 2.5 cm/s is 5.5 cm which in good agreement with the experimental measurement. The inclusion of cohesive forces of 5- and 10-particle-weight slightly increases the bed expansion to about 5.8 cm ~~as can be seen in Figure 11~~. Overall, the bed height is predicted by the current simulations very well. ~~with~~ This is different from the ~~no~~ significant over-prediction of bed height for Group A particles ~~as~~ reported in the literature.

5. Conclusion

The current study reports an effort to model the fluidization behavior of Geldart's group A particles using CFD-DEM simulations. For this purpose, experimental tests of two types of Group A particles in a small scale pseudo-2D fluidized bed facility were conducted. Three-dimensional MFIX-DEM simulations were carried out to validate against the experimental data. To the authors' best knowledge, this is the first study reporting direct comparison of detailed flow hydrodynamics between CFD-DEM simulation and experiment for group A particles in a fluidized bed.

For large FCC particles tested in the current study which is close to the transition from Group A to Group B, the numerical simulations using non-cohesive particles reasonably predicted the bed

expansion and bubble characteristics comparing to the experimental measurements and observation. Incorporation of cohesive inter-particle force, i.e. van der Waals force, into the DEM simulation altered the flow behavior gradually as the strength was increased. DEM simulations with strong cohesive van der Waals force are capable of predicting the agglomerating phenomenon observed in the experimental tests. However, the simulations tend to predict larger agglomerates with smaller aspect ratio comparing to the small elongated agglomerates~~However, simply including the cohesive force in DEM calculation was not able to predict the agglomerates~~ of particles observed in the experimental high-speed videos. It is believed that the gas-solid interaction plays a ~~key~~ significant role in the formation of agglomerates with the presence of cohesive interparticle forces.

For ~~the~~ NETL-32D sorbent particles which are light and small, the cohesive forces tested had a stronger impact on the solid circulation pattern. It is necessary to include the cohesive force in order to predict realistic bubbling pattern and solid circulation. A layer of particles sticking on the wall observed in the experimental tests was captured by the simulations with cohesive force. Finally, ~~the CFD-DEM simulations were able to predict the bed expansion reasonably well with and without the cohesive force.~~ the predicted bed expansion shows reasonably good comparison with the experiment and was found insensitive to the adhesion force.

Acknowledgements

This technical effort was performed in support of the U.S. Department of Energy, Office of Fossil Energy's Carbon Capture Simulation Initiative (CCSI) and Advanced Numerical Simulation of Multiphase Flow through the National Energy Technology Laboratory under the RES contract DE-FE0004000.

Reference

[1] D. Geldart, Types of gas fluidization, Powder Technol. 7 (1973) 285–292. doi:10.1016/0032-5910(73)80037-3.

[2] D. Gidaspow, L. Huilin, Equation of state and radial distribution functions of FCC particles in a CFB, AIChE J. 44 (1998) 279–293. doi:10.1002/aic.690440207.

[3] S. Karimipour, T. Pugsley, Study of gas streaming in a deep fluidized bed containing Geldart's Group A particles, Chem. Eng. Sci. 65 (2010) 3508–3517. doi:10.1016/j.ces.2010.02.045.

[4] T. McKeen, T. Pugsley, Simulation and experimental validation of a freely bubbling bed of FCC catalyst, Powder Technol. 129 (2003) 139–152. doi:10.1016/S0032-5910(02)00294-2.

[5] H. Cui, Effects of temperature on local two-phase flow structure in bubbling and turbulent fluidized beds of FCC particles, Chem. Eng. Sci. 59 (2004) 3413–3422. doi:10.1016/j.ces.2004.05.006.

[6] J.R. Grace, T. Li, Complementarity of CFD, experimentation and reactor models for solving challenging fluidization problems, Particuology. 8 (2010) 498–500. doi:10.1016/j.partic.2010.09.003.

[7] D. Gidaspow, Multiphase Flow and Fluidization: Continuum and Kinetic Theory Descriptions, Academic Press, 1994.

[8] N.G.G. Deen, M. Van Sint Annaland, M.A. Van der Hoef, J.A.M.A.M. Kuipers, M.V.S. Annaland, M.A. Van Der Hoef, et al., Review of discrete particle modeling of fluidized beds, Chem. Eng. Sci. 62 (2007) 28–44. doi:10.1016/j.ces.2006.08.014.

[9] D.M. Snider, An Incompressible Three-Dimensional Multiphase Particle-in-Cell Model for Dense Particle Flows, J. Comput. Phys. 170 (2001) 523–549. doi:10.1006/jcph.2001.6747.

[10] J.K. Pandit, X.S. Wang, M.J. Rhodes, On Geldart Group A behaviour in fluidized beds with and without cohesive interparticle forces : A DEM study, 164 (2006) 130–138. doi:10.1016/j.powtec.2006.03.007.

[11] T. Mckeen, T.S. Pugsley, Simulation of Cold Flow FCC Stripper Hydrodynamics at

Small Scale Using Computational Fluid Dynamics Simulation of Cold Flow FCC Stripper Hydrodynamics at Small Scale Using Computational Fluid Dynamics, Int. J. Chem. React. Eng. (2003).

[12] S. Zimmermann, F. Taghipour, CFD Modeling of the Hydrodynamics and Reaction Kinetics of FCC Fluidized-Bed Reactors, Ind. Eng. Chem. Res. 44 (2005) 9818–9827. doi:10.1021/ie050490+.

[13] T. Li, K. Pougatch, M. Salcudean, D. Grecov, Numerical simulation of horizontal jet penetration in a three-dimensional fluidized bed, Powder Technol. 184 (2008) 89–99. doi:10.1016/j.powtec.2007.08.007.

[14] X. Liu, C. Zhu, S. Geng, M. Yao, J. Zhan, G. Xu, Two-fluid modeling of Geldart A particles in gas–solid micro-fluidized beds, Particuology. 21 (2015) 118–127. doi:10.1016/j.partic.2014.05.012.

[15] B. van Wachem, S. Sasic, Derivation, simulation and validation of a cohesive particle flow CFD model, AIChE J. 54 (2008) 9–19. doi:10.1002/aic.11335.

[16] A.H.A. Motlagh, J.R. Grace, M. Salcudean, C.M. Hrenya, New structure-based model for Eulerian simulation of hydrodynamics in gas–solid fluidized beds of Geldart group “A” particles, Chem. Eng. Sci. 120 (2014) 22–36. doi:10.1016/j.ces.2014.08.042.

[17] J. Wang, M. Vanderhoef, J. Kuipers, Why the two-fluid model fails to predict the bed expansion characteristics of Geldart A particles in gas-fluidized beds: A tentative answer, Chem. Eng. Sci. 64 (2009) 622–625. doi:10.1016/j.ces.2008.09.028.

[18] W. Wang, J. Li, Simulation of gas–solid two-phase flow by a multi-scale CFD approach—of the EMMS model to the sub-grid level, Chem. Eng. Sci. 62 (2007) 208–231. doi:10.1016/j.ces.2006.08.017.

[19] Y. Igci, A.T.A. Iv, S. Sundaresan, T.O. Brien, A.T. Andrews IV, S. Sundaresan, et al., Filtered two-fluid models for fluidized gas-particle suspensions, AIChE J. 54 (2008) 1431–1448. doi:10.1002/aic.11481.

[20] J.-F. Parmentier, O. Simonin, O. Delsart, A functional subgrid drift velocity model for filtered drag prediction in dense fluidized bed, AIChE J. 58 (2012) 1084–1098. doi:10.1002/aic.12647.

[21] T. Li, J. Dietiker, W. Rogers, R. Panday, B. Gopolan, G. Breault, Investigation of CO2 capture using solid sorbents in a fluidized bed reactor: cold flow hydrodynamics, Powder Technol. 301 (2016) 1130–1143.

[22] A. Yu, B. Xu, Particle-scale modelling of gas-solid flow in fluidisation, J. Chem. Technol. Biotechnol. 78 (2003) 111–121. doi:10.1002/jctb.788.

[23] M. Ye, M.A. van der Hoef, J.A.M. Kuipers, M. Vanderhoef, J.A.M. Kuipers, The effects of particle and gas properties on the fluidization of Geldart A particles, Chem. Eng. Sci. 60 (2005) 4567–4580. doi:10.1016/j.ces.2005.03.017.

[24] M. Ye, M.. van der Hoef, J.A.. Kuipers, A numerical study of fluidization behavior of Geldart A particles using a discrete particle model, Powder Technol. 139 (2004) 129–139. doi:10.1016/j.powtec.2003.10.012.

[25] J. Pandit, X. Wang, M. Rhodes, Study of Geldart's Group A behaviour using the discrete element method simulation, Powder Technol. 160 (2005) 7–14. doi:10.1016/j.powtec.2005.04.044.

[26] T. Kobayashi, T. Tanaka, T. Kawaguchi, T. Mukai, Y. Tsuji, DEM Analysis on Flow Patterns of Geldart's Group A Particles in Fluidized Bed-Effect of Adhesion and Lubrication Forces-, J. Soc. Powder Technol. Japan. 43 (2006) 737–745. doi:10.4164/sptj.43.737.

[27] Q.F. Hou, Z.Y. Zhou, A.B. Yu, Micromechanical modeling and analysis of different flow regimes in gas fluidization, Chem. Eng. Sci. 84 (2012) 449–468. doi:10.1016/j.ces.2012.08.051.

[28] O. Molerus, Interpretation of Geldart's type A, B, C and D powders by taking into account interparticle cohesion forces, Powder Technol. 33 (1982) 81–87. doi:10.1016/0032-5910(82)85041-9.

[29] R. Moreno-Atanasio, B.H. Xu, M. Ghadiri, Computer simulation of the effect of contact stiffness and adhesion on the fluidization behaviour of powders, Chem. Eng. Sci. 62 (2007) 184–194. doi:10.1016/j.ces.2006.08.036.

[30] T. Kobayashi, T. Tanaka, N. Shimada, T. Kawaguchi, DEM–CFD analysis of fluidization behavior of Geldart Group A particles using a dynamic adhesion force model, Powder Technol. 248 (2013) 143–152. doi:10.1016/j.powtec.2013.02.028.

[31] Y. Gu, A. Ozel, S. Sundaresan, A modified cohesion model for CFD–DEM simulations of fluidization, Powder Technol. (2015). doi:10.1016/j.powtec.2015.09.037.

[32] J.E. Galvin, S. Benyahia, The effect of cohesive forces on the fluidization of aeratable powders, AIChE J. 60 (2014) 473–484. doi:10.1002/aic.14307.

[33] P. Liu, C.Q. LaMarche, K.M. Kellogg, C.M. Hrenya, Fine-particle defluidization: Interaction between cohesion, Young's modulus and static bed height, Chem. Eng. Sci. 145 (2016) 266–278. doi:10.1016/j.ces.2016.02.024.

[34] D.J. Fauth, M.L. Gray, H.W. Pennline, H.M. Krutka, S. Sjostrom, a. M. Ault, Investigation of porous silica supported mixed-amine sorbents for post-combustion CO 2 capture, Energy and Fuels. 26 (2012) 2483–2496. doi:10.1021/ef201578a.

[35] S. Choi, M.L. Gray, C.W. Jones, Amine-tethered solid adsorbents coupling high adsorption capacity and regenerability for CO2 capture from ambient air., ChemSusChem. 4 (2011) 628–35. doi:10.1002/cssc.201000355.

[36] J.R. Tucker, L.J. Shadle, S. Benyahia, J. Mei, C. Guenther, M.E. Koepke, Improvement in Precision, Accuracy, and Efficiency in Standardizing the Characterization of Granular Materials, in: Vol. 7A Fluids Eng. Syst. Technol., ASME, 2013: p. V07AT08A064. doi:10.1115/IMECE2013-65027.

[37] F. Shaffer, B. Gopalan, R.W. Breault, R. Cocco, S.B.R. Karri, R. Hays, et al., High speed imaging of particle flow fields in CFB risers, Powder Technol. 242 (2013) 86–99. doi:10.1016/j.powtec.2013.01.012.

[38] R. Garg, J. Galvin, T. Li, S. Pannala, Documentation of open-source MFIX-DEM software for gas-solids flows., (2010).

[39] P.A. Cundall, O.D.L. Strack, A discrete numerical model for granular assemblies, Géotechnique. 29 (1979) 47–65. doi:10.1680/geot.1979.29.1.47.

[40] Y. Tsuji, T. Kawaguchi, T. Tanaka, Discrete particle simulation of two-dimensional fluidized bed, Powder Technol. 77 (1993) 79–87. doi:10.1016/0032-5910(93)85010-7.

[41] T. Li, R. Garg, J. Galvin, S. Pannala, Open-source MFIX-DEM software for gas-solids flows: Part II — Validation studies, Powder Technol. 220 (2012) 138–150. doi:10.1016/j.powtec.2011.09.020.

[42] R. Garg, J. Galvin, T. Li, S. Pannala, Open-source MFIX-DEM software for gas–solids flows: Part I—Verification studies, Powder Technol. 220 (2012) 122–137. doi:10.1016/j.powtec.2011.09.019.

[43] T. Li, P. Gopalakrishnan, R. Garg, M. Shahnam, CFD–DEM study of effect of bed thickness for bubbling fluidized beds, Particuology. 10 (2012) 532–541. doi:10.1016/j.partic.2012.02.006.

[44] P. Gopalakrishnan, D. Tafti, Development of parallel DEM for the open source code MFIX, Powder Technol. 235 (2013) 33–41. doi:10.1016/j.powtec.2012.09.006.

[45] H. Liu, D.K. Tafti, T. Li, Hybrid parallelism in MFIX CFD-DEM using OpenMP, Powder Technol. 259 (2014) 22–29. doi:10.1016/j.powtec.2014.03.047.

[46] J.N. Israelachvili, Intermolecular and Surface Forces, Elsevier, 2011. doi:10.1016/B978-0-12-375182-9.10006-5.

[47] J.F. de Jong, S.O. Odu, M.S. van Buijtenen, N.G. Deen, M. van Sint Annaland, J.A.M. Kuipers, Development and validation of a novel Digital Image Analysis method for fluidized bed Particle Image Velocimetry, Powder Technol. 230 (2012) 193–202. doi:10.1016/j.powtec.2012.07.029.

[48] Y. Gu, S. Chialvo, S. Sundaresan, Rheology of cohesive granular materials across multiple dense-flow regimes, Phys. Rev. E. 90 (2014) 032206. doi:10.1103/PhysRevE.90.032206.

[49] J. Seville, Interparticle forces in fluidisation: a review, Powder Technol. 113 (2000) 261–268. doi:10.1016/S0032-5910(00)00309-0.

[50] T. Li, J. Grace, X. Bi, Study of wall boundary condition in numerical simulations of bubbling fluidized beds, Powder Technol. 203 (2010) 447–457. doi:10.1016/j.powtec.2010.06.005.

LIST OF FIGURES

Formatted: Default Paragraph Font, Check spelling and grammar

Formatted: Default Paragraph Font, Check spelling and grammar

Formatted: Default Paragraph Font, Check spelling and grammar

Formatted: Default Paragraph Font, Check spelling and grammar

Formatted: Default Paragraph Font, Check spelling and grammar

Formatted: Default Paragraph Font, Check spelling and grammar

Formatted: Default Paragraph Font, Check spelling and grammar

Formatted: Default Paragraph Font, Check spelling and grammar

Formatted: Default Paragraph Font, Check spelling and grammar

Formatted: Default Paragraph Font, Check spelling and grammar

Formatted: Default Paragraph Font, Check spelling and grammar

Formatted: Default Paragraph Font, Check spelling and grammar

Formatted: Default Paragraph Font, Check spelling and grammar

Formatted: Default Paragraph Font, Check spelling and grammar

Formatted: Default Paragraph Font, Check spelling and grammar

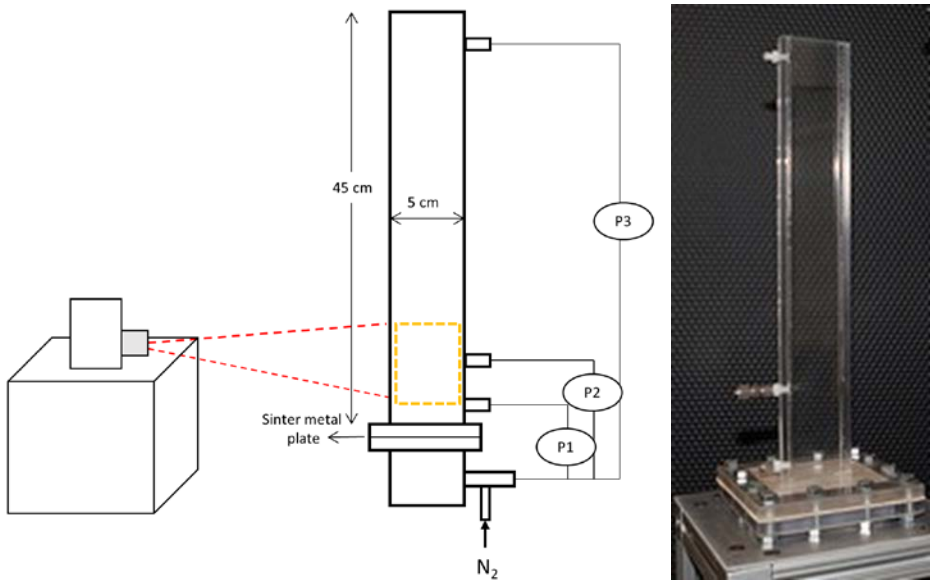

(a) (b)

Figure 1. (a) Schematic and (b) picture of the experimental setup

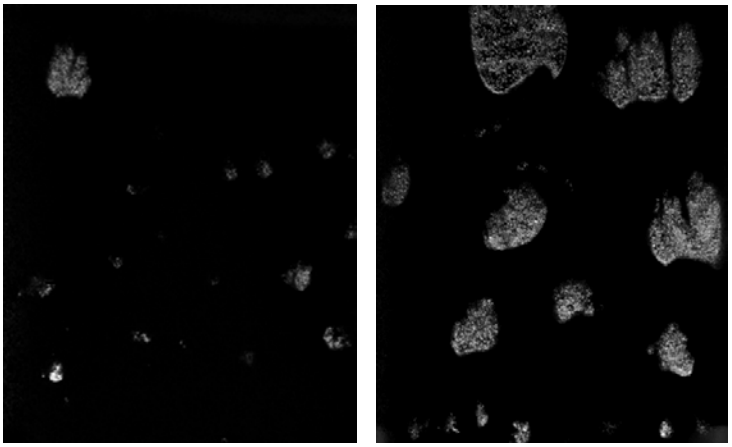

(a) (b)

Figure 2. Raw images of bubbling fluidized bed of FCC particles with superficial gas velocities of (a) 2Umf; (b) 5Umf (static bed height: 6 cm).

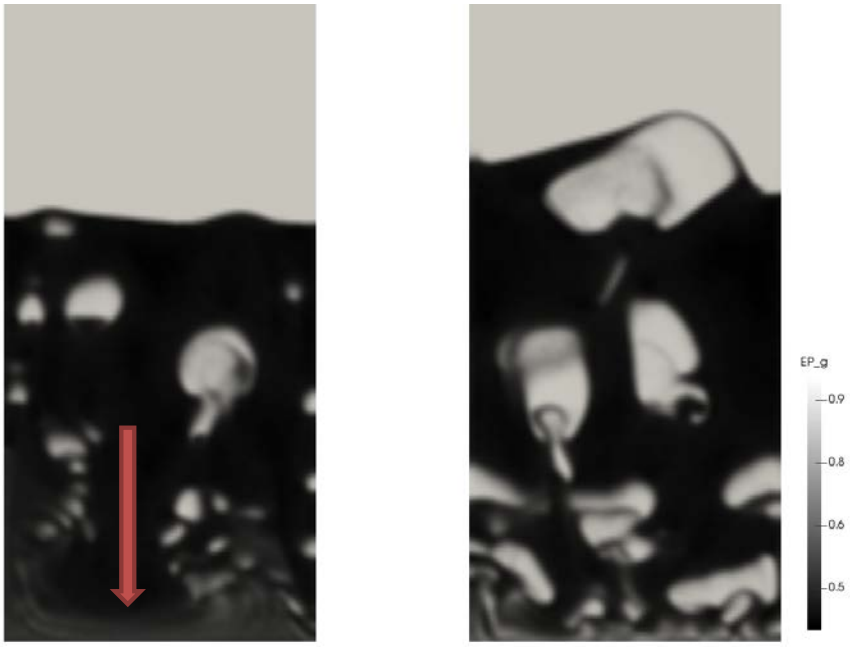

(a) (b)

Figure 3. Snapshots of numerical simulations of FCC particles with superficial gas velocities of (a) 2Umf; (b) 5Umf (static bed height: 6 cm).

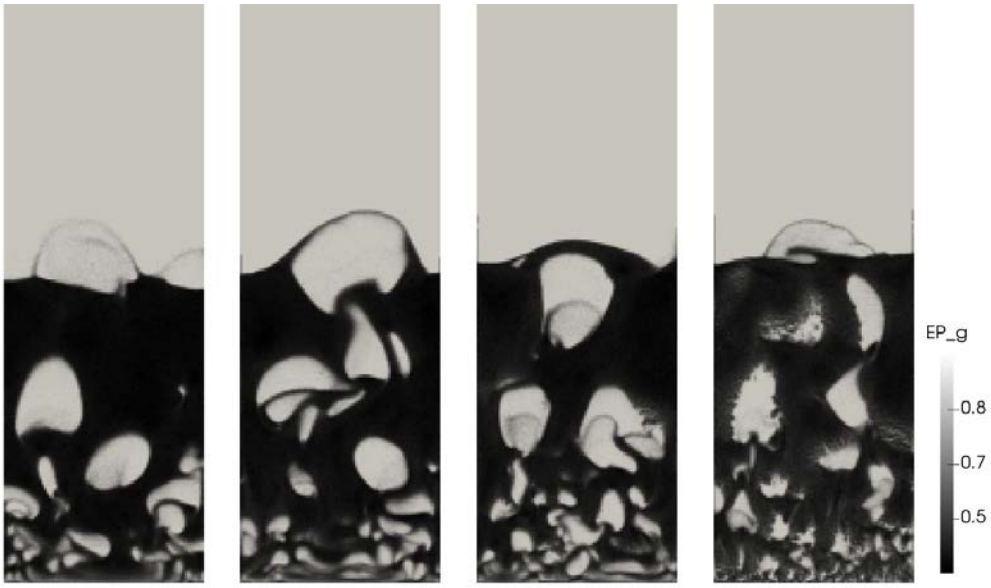

(a)

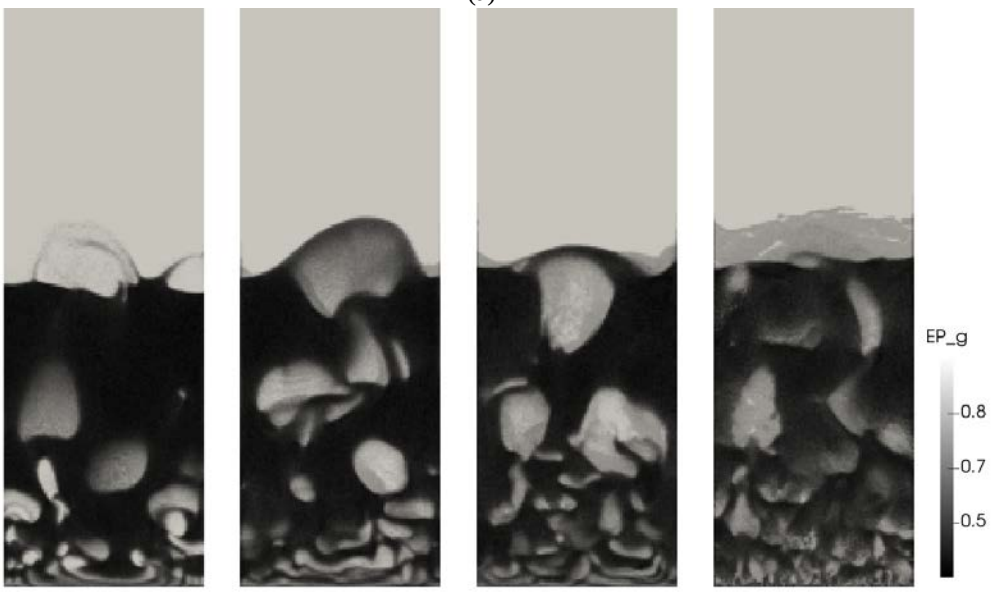

(b)

Figure 4. Effect of cohesive force on the instantaneous bubbling behavior of FCC particles under 5Umf for (a) central slice and (b) the front wall ($F_{vdw,\max}/W_p$ = 0, 5, 10, and 20 from left to right).

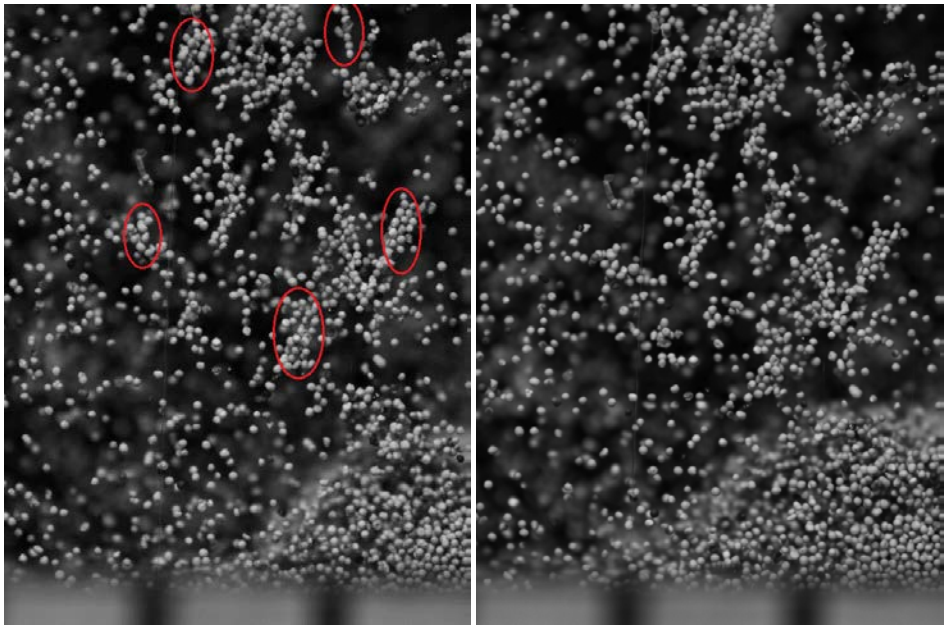

(a) (b)

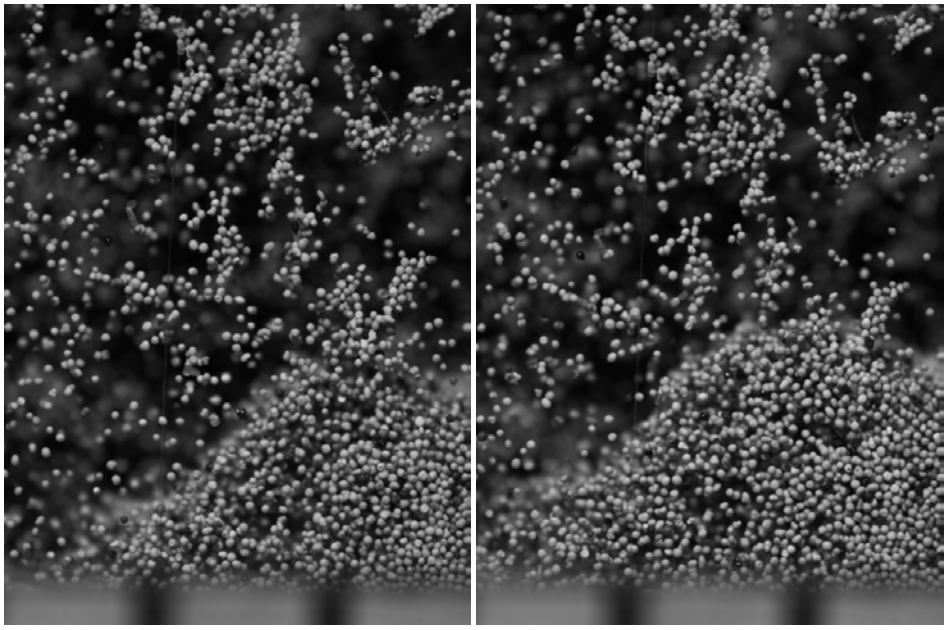

(c) (d)

Figure 5. Pictures taken for FCC particles with 5Umf (time interval between images is 0.002 second).

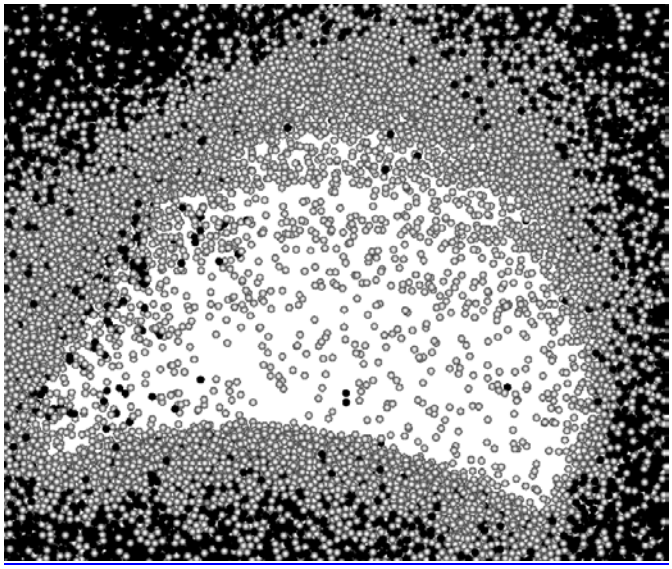

(a)

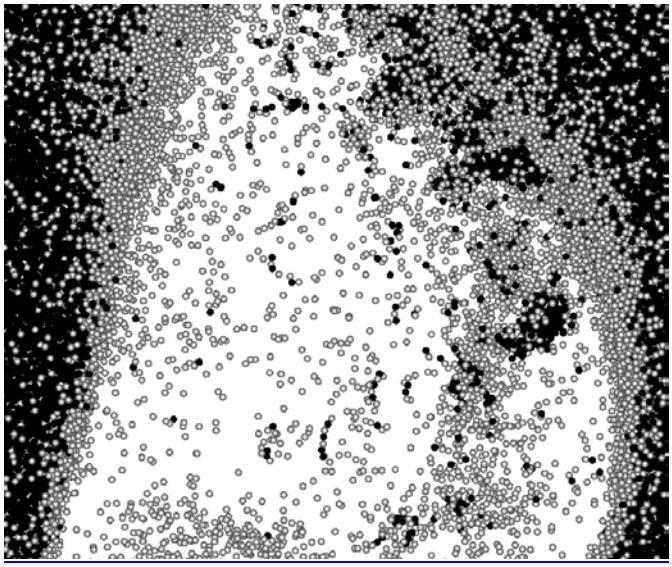

(b)

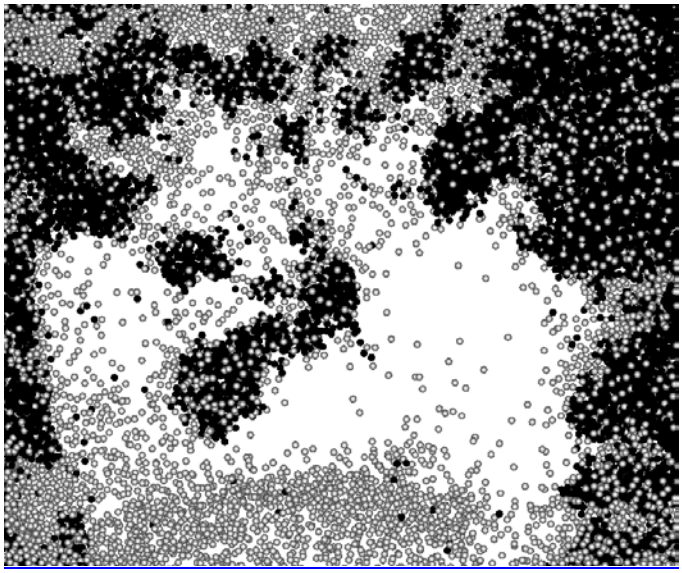

(c)

Figure 6. Snapshots of DEM simulations characterizing agglomerates formation for different strengths of cohesive force (a) $F_{vdw,\max}/W_p$ = 5, (b) $F_{vdw,\max}/W_p$ = 10, (c) $F_{vdw,\max}/W_p$ = 20.

Field Code Changed
Field Code Changed
Field Code Changed

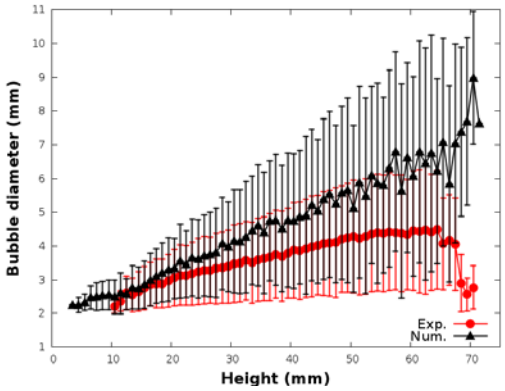
Bubble diameter (mm)
Height (mm)
Exp.
Num.

(a)

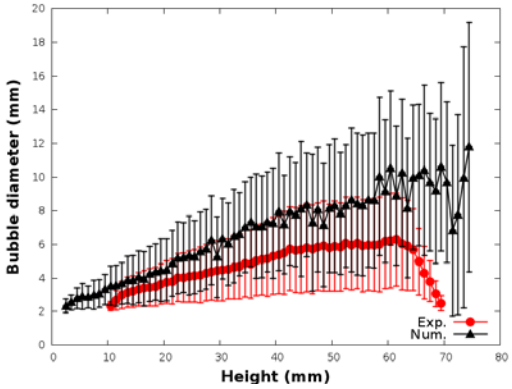
Bubble diameter (mm)
Height (mm)
Exp.
Num.

(b)

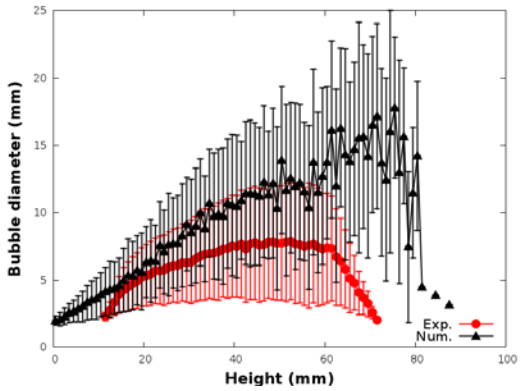

(c)

Figure 7. Comparison of bubble diameter along the bed height for (a) 2 Umf; (b) 3 Umf; (c) 5 Umf (error bar corresponds to the standard deviation, numerical results are for non-cohesive particles).

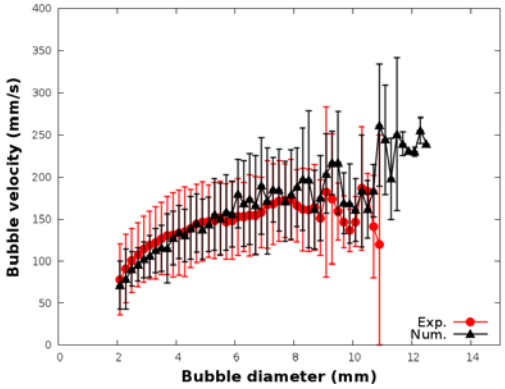
Bubble velocity (mm/s)
Bubble diameter (mm)
Exp.
Num.

(a)

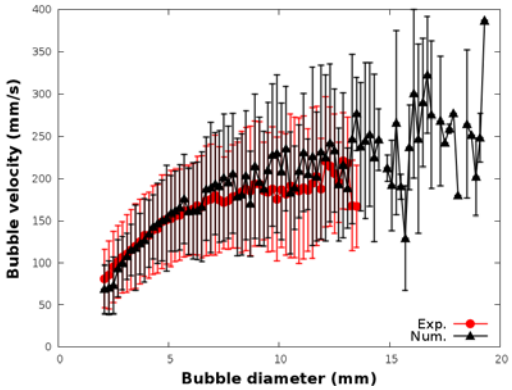
Bubble velocity (mm/s)
Bubble diameter (mm)
Exp.
Num.

(b)

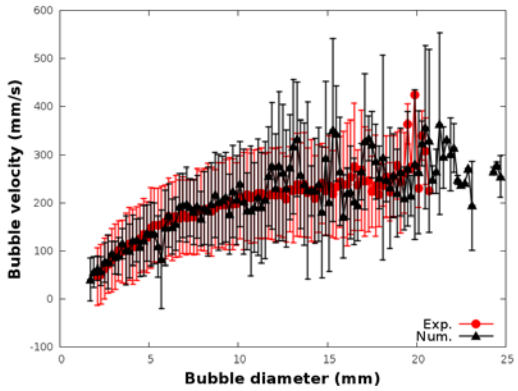

(c)

Figure 8. Comparison of vertical bubble velocity as a function of bubble diameter for (a) 2 Umf; (b) 3 Umf; (c) 5 Umf (error bar corresponds to the standard deviation, numerical results are for non-cohesive particles).

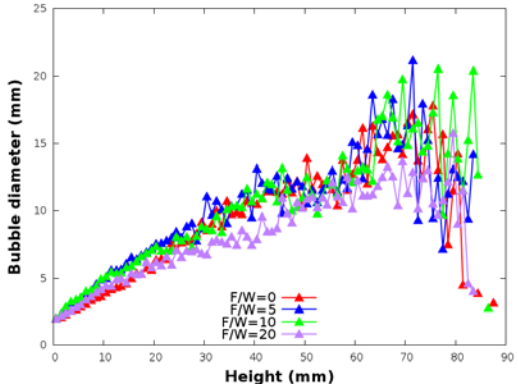

(a)

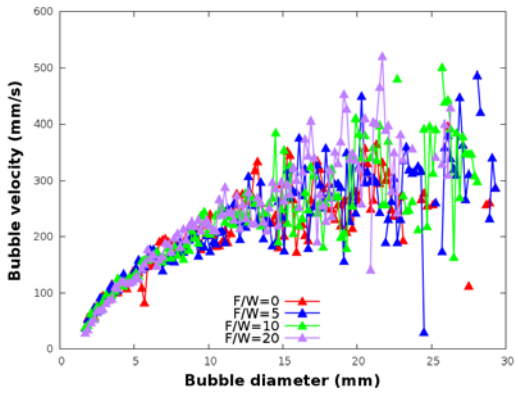

(b)

Figure 9. Effect of cohesive force on (a) mean bubble diameter along the bed height and (b) vertical bubble velocity as a function of bubble diameter for the case of 5 Umf.

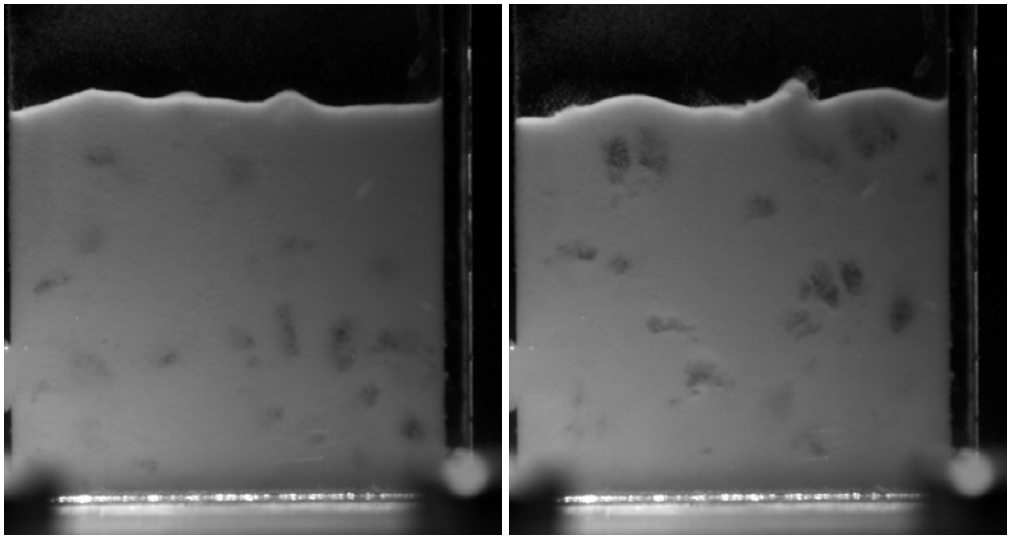

(a) (b)

Figure 10. Experimental images of 32D sorbent particles with superficial gas velocity of (a) 1.5 cm/s; (b) 2.5 cm/s.

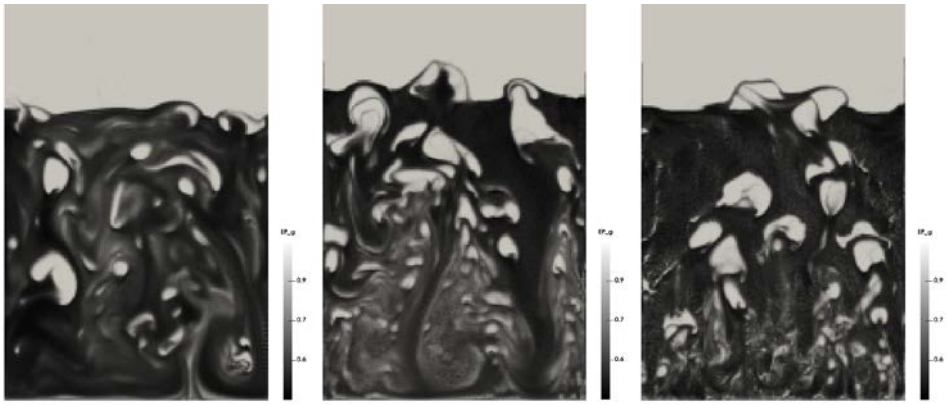

(a)

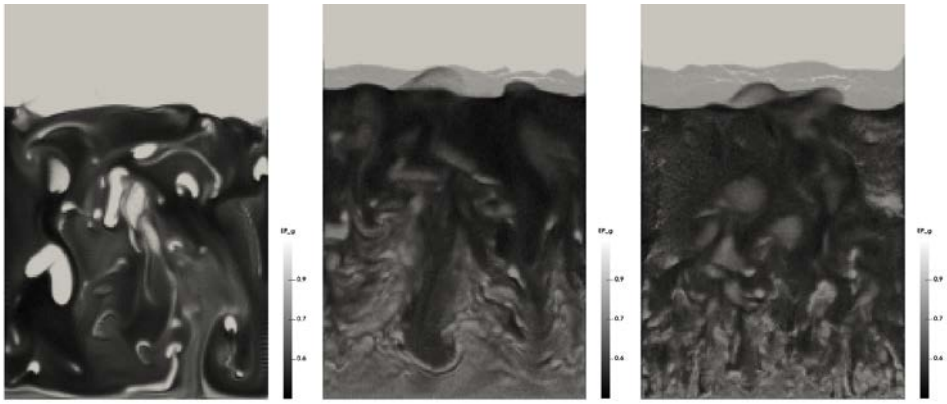

(b)

Figure 11. Effect of cohesive force on the instantaneous bubbling behavior of 32D sorbent particles with a superficial gas velocity of 2.5 cm/s for (a) central slice and (b) front wall ($F_{vdw,\max}/W_p$ = 0, 5, 10 from left to right).

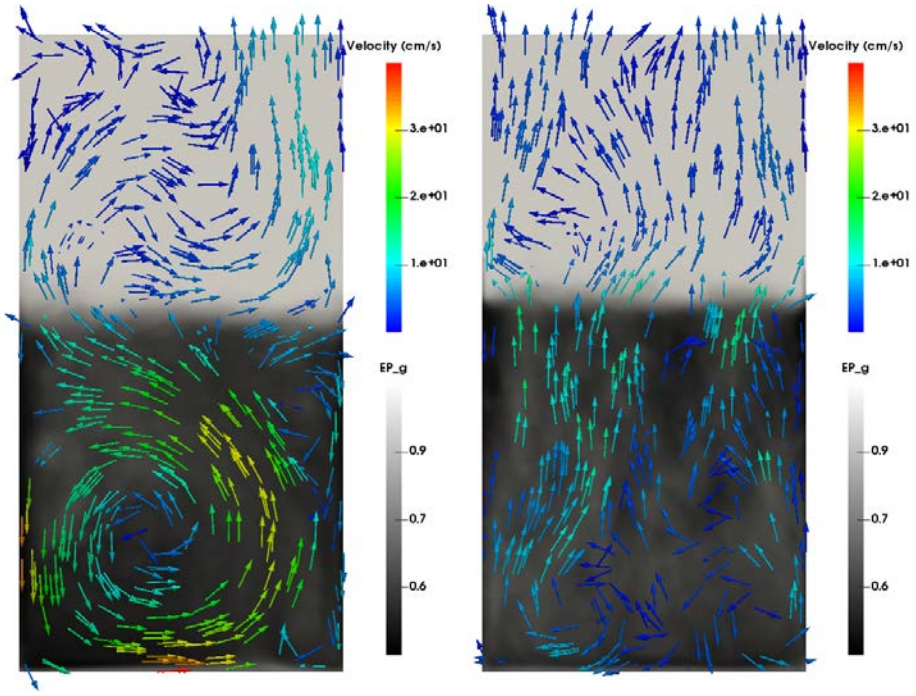

(a) (b)

Figure 12. Distribution of mean voidage and gas velocity vectors along the central slice (a) $F_{vdw,\max}/W_p = 0$; (b) $F_{vdw,\max}/W_p = 5$.

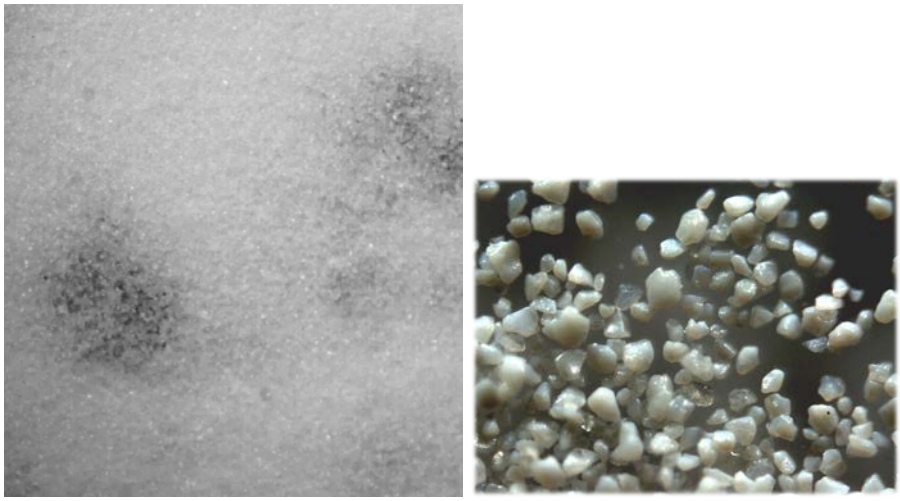

(a) (b)

Figure 13. Close view of the experimental test of 32D sorbents with a superficial gas velocity of 2.5 cm/s with dark color indicates high voidage (a) and photomicrograph of 32D sorbent particles (b).

LIST OF TABLES

Table 1. Numerical parameters used in the simulations.

Gas properties			
Pressure (Pa)	1.01~~e5~~x10^{5}	Temperature (K)	298
Viscosity (Pa.s)	1.8 x10^{-5}~~e-5~~	Molecular weight (kg/kmol)	~~29~~ 28
FCC particles			
Diameter (µm)	148	Density (kg/m^{3})	1300
Particle-particle friction coefficient (-)	0.3	Particle-wall friction coefficient (-)	0.3
Particle-particle restitution coefficient (-)	0.97	Particle-wall restitution coefficient (-)	0.97
Spring constant (N/m)	5	Minimum fluidization velocity, Umf (cm/s)	1.73
Width (cm)	5.08	Cell count	84
Height (cm)	15	Cell count	250
Thickness (cm)	0.32	Cell count	6
Solid time step (s)	3.8 x10^{-6}		
NETL-32D sorbent			
Diameter (µm)	100	Density (kg/m^{3})	480
Particle-particle friction coefficient (-)	0.3	Particle-wall friction coefficient (-)	0.3
Particle-particle restitution coefficient (-)	0.97	Particle-wall restitution coefficient (-)	0.97
Spring constant (N/m)	5	Minimum fluidization velocity, Umf (cm/s)	0.23
Width (cm)	5.08	Cell count	127
Height (cm)	10	Cell count	250
Thickness (cm)	0.32	Cell count	8
Solid time step (s)	1.2 x10^{-6}		

Table 2. Comparison of bed expansion for FCC particles with a static bed height of 6 cm predicted by CFD-DEM simulations ~~of non-cohesive particles~~.

~~Superficial gas velocity~~Condition	Experiment (cm)~~al bed height (cm)~~	Prediction $F_{vdw,\max}/W_p = 0$	Prediction $F_{vdw,\max}/W_p =$ 5~~Predicted bed height (cm)~~
2 Umf	6.7	6.9	7.1~~6.9~~
3 Umf	7~7.3	7.2	~~7.2~~
5 Umf	7.9~8.2	7.9	8.2~~7.9~~

Formatted: Font color: Red
Formatted Table
Field Code Changed
Formatted: Font color: Red
Field Code Changed
Formatted: Font color: Red
Formatted: Font color: Red
Formatted: Font color: Red